BIOACTIVE GLASS COATINGS FOR ORTHOPEDIC METALLIC IMPLANTS

S. Lopez-Esteban,[1] E. Saiz,[1] S. Fujino,[2] T. Oku,[3] K. Suganuma,[3] and A. P. Tomsia[1]

[1]Lawrence Berkeley National Laboratory, Berkeley, CA 94720, USA
[2]Kyushu University, Kasuga-shi, Fukuoka 816-8580, Japan.
[3]Institute of Scientific and Industrial Research, Osaka University, Osaka 567-0047, Japan

---

Corresponding author: Dr. Sonia Lopez-Esteban
Materials Sciences Division
Lawrence Berkeley National Laboratory, Berkeley, CA 94720
USA
Phone: 510-486-4817, FAX: 510-486-4761
e-mail: slopez-esteban@lbl.gov

Bioactive glass coatings for orthopedic metallic implants

S. Lopez-Esteban,[1] E. Saiz,[1] S. Fujino,[2] T. Oku,[3] K. Suganuma,[3] and A. P. Tomsia[1]

[1]*Lawrence Berkeley National Laboratory, Berkeley, CA 94720, USA*
[2]*Kyushu University, Kasuga-shi, Fukuoka 816-8580, Japan.*
[3]*Institute of Scientific and Industrial Research, Osaka University, Osaka 567-0047, Japan*

Abstract

The objective of this work is to develop bioactive glass coatings for metallic orthopedic implants. A new family of glasses in the SiO_2-Na_2O-K_2O-CaO-MgO-P_2O_5 system has been synthesized and characterized. The glass properties (thermal expansion, softening and transformation temperatures, density and hardness) are in line with the predictions of established empirical models. The optimized firing conditions to fabricate coatings on Ti-based and Co-Cr alloys have been determined and related to the glass properties and the interfacial reactions. Excellent adhesion to alloys has been achieved through theformation of 100–200 nm thick interfacial layers (Ti_5Si_3 on Ti-based alloys and CrO_x on Co-Cr). Finally, glass coatings, approximately 100 μm thick, have been fabricated onto commercial Ti alloy-based dental implants.

Key Words: Films (A), interfaces (B), thermal expansion (C), glass (D), biomedical applications (E).

I. Introduction

Since the discovery of Bioglass® by Hench, bioactive glasses have been used in many medical applications, such as drug delivery systems, non-load-bearing implants, and bone cements. [1-3] However, due to their poor mechanical properties, these glasses cannot be

used in load-bearing applications, where metallic alloys are still the materials of choice. It was recognized early on that one of the main applications of bioactive glasses could be coatings for prosthetic metallic implants.[4] These coatings would serve two purposes: improving the osseointegration of the implants, and protecting the metal against corrosion from the body fluids and the tissue from the corrosion products of the alloys. Unfortunately, most of the attempts to coat metallic implants with bioactive glasses have had limited success. This is due to poor adhesion of the coating and/or degradation of the glass properties during the coating procedure (typically enameling, or flame or plasma spray coating).[4]

Several key design criteria are necessary for the successful development of new bioactive coatings for implants: (1) the firing cycle should not degrade the properties of the metal or the glass; (2) the thermal expansion of the glass and the metal should be similar in order to avoid the generation of large thermal stresses that can result in coating cracking or delamination during fabrication (typically it is preferred that the coating has a slightly lower thermal expansion than the metal, resulting in small compressive stresses); (3) the firing cycles should result in interfaces with optimum adhesion; and (4) the glass coatings should form hydroxyapatite when in contact with body fluids. The Ti alloys used in the fabrication of prosthetic implants are very reactive, and the glass/metal reactions that occur during firing are detrimental to adhesion and bioactivity. Thus, coating titanium with bioactive glasses is challenging. Additionally, firing temperatures below the $\alpha \rightarrow \beta$ transformation of Ti (between 885 and 950°C for unalloyed Ti, depending on the impurity content,[5-6] and between 955 and 1010°C for Ti6Al4V[6]) are required to avoid a degradation of the mechanical properties of the implant. Bioactive

glasses are typically silicate glasses with silica content below 60 wt%. Most of these glasses are hygroscopic and crystallize readily at the firing temperatures required for enameling. The thermal expansion coefficients of bioactive glasses are typically much larger than those of Ti alloys. The simplest way to reduce thermal expansion is to increase the SiO_2 content of the glass; unfortunately, this is at the expense of bioactivity, which is significantly reduced.[1-3]

This work examines the properties of a new family of bioactive glasses designed to coat Ti-based alloys. The results are compared with existing models for calculating properties of silicate glasses and with the optimum enameling conditions needed for the fabrication of bioactive coatings on Ti-based and Co-Cr alloys with good adhesion to the metal.

II. Experimental

Glasses in the system SiO_2-Na_2O-K_2O-CaO-MgO-P_2O_5 were prepared by mixing SiO_2 (99.5%)*, $CaCO_3$ (99.9%)**, MgO (98.6%)**, K_2CO_3 (99%)#, $NaHCO_3$ (99.5%)** and $NaPO_3$ (99.7%)# in ethanol using a high-speed stirrer. The compositions of the glasses are summarized in Table 1. The mixtures were dried at 80°C for 12 h and then fired in air at 1400–1500°C for 4 h in a Pt crucible (glasses with larger silica contents were fired at higher temperatures). The melt was cast into a graphite mold to obtain glass plates (~50 × 50 × 5 mm) that were subsequently annealed at 500°C for 6 h to relieve stresses. The thermal expansion (α), softening (T_s), and transformation (T_g) temperatures were measured in a calibrated dilatometer with an alumina holder and push rod, using glass

*Cerac, USA.
**JT Baker, USA.
#Allied Chemical, USA

bars 25 × 3 × 3 mm. The Vickers hardness was evaluated using loads between 0.5 and 1.2 kg in ambient air. The density of the glasses was measured using the Archimedes method.

To manufacture the coatings, the glass was milled in a planetary agate mill. After milling, the glass particle size was measured using a sedimentation technique. A suspension of the glass powder in ethanol was deposited on flat metallic substrates ~10 × 10 × 1 mm (Ti, Ti6Al4V, or Vitallium®, a Co-Cr alloy), which had been previously polished with diamond (1 μm particle size) and cleaned in acetone and ethanol. Additionally, suspensions of the glass powders in ethanol with a 50–75 wt% solid content were used to coat cylindrical Ti6AlV samples (1 mm radius, 10 mm long) and titanium internal hexagonal cylinder implants (3.3 mm diameter and 10 mm length, 3i Implant Innovation) by dip coating, using coating speeds up to 1,000 mm/min. The dip-coating suspensions were prepared using a magnetic stirrer. The solution was continuously stirred between immersions in order to avoid settling of the powders, and the glass powders were analyzed by Fourier Transform Infrared Spectroscopy (FTIR).

The resulting coatings were dried in air at 75°C for 12 hr, and fired in air at temperatures ranging between 650 and 850°C to make the glass flow and adhere to the metal. The specimens were introduced in the furnace previously preheated to 600–650°C and heated at 40°C/min. to the desired temperature. During heating, the furnace was evacuated to 0.1 atm. Once the maximum temperature was reached, air was let into the chamber. After the required time, they were quenched in air. The final coating thickness ranged from 25 to 150 μm.

The crystallization of the coatings was evaluated by x-ray diffraction (XRD). The

surfaces of the coatings, as well as polished cross sections, were examined by optical microscopy and scanning electron microscopy with associated energy dispersive spectroscopy analysis (SEM-EDS). The glass/metal interfaces were also analyzed using transmission electron microscopy (TEM). Samples for TEM were prepared by cutting cross sections of the glass/alloy interface. The sections were ground to a thickness of ~100 μm with emery paper, and then fixed into a Cu mesh with a 3 mm diameter. The disks were polished with a dimple grinder (Gatan, Model 656) to less than 20 μm in thickness and milled by argon-ion milling. TEM observations were performed with a 1250 kV electron microscope (an ARM 1250) having a point-to-point resolution of 0.12 nm, and in a FEI TECNAI 20 electron microscope operated at 200 kV. Chemical analysis of the interface was performed using electron probe microanalysis (EPMA). In the elemental line analysis, the focused incident beam (~4 nm diameter) was positioned across the glass/alloy interface, and an x-ray spectrum was acquired for 1 s at each position.

In order to study the adherence of the coatings, the relative crack resistance was qualitatively evaluated by indentation. Indentation testing is an attractive alternative to more costly fracture mechanics experiments for determining adhesion between two materials. Vickers indentations on the coating surfaces were performed in air, with loads of up to 6.2 kg. Indentations on the coatings and glass/metal interfaces were also performed on polished cross sections, using loads ranging from 0.05 to 1.2 kg. The path of the cracks produced during the indentation (along the glass/metal interface or through the glass coating) provides a qualitative assessment of the adhesion between phases. However, because of the complex loading situations involved, it is recognized that a more

exhaustive characterization is needed to predict the *in vivo* response of the interfaces.

The behavior of selected glass coatings in simulated body fluid (SBF) was studied by *in vitro* tests. The specimens (15 × 10 × 1 mm) were soaked for up to 30 days in 20 ml of SBF at a constant temperature of 36.5°C. After soaking, the coatings were rinsed in distilled water, dried, and analyzed by XRD, SEM-EDS, and Fourier Transform Infrared Spectromicroscopy (FTIRSM) at the Lawrence Berkeley National Laboratory Advanced Light Source (ALS).

III. Results and Discussion

(1) Glass properties

XRD analysis of the synthesized glasses did not show any crystalline phase, with the exception of 6P64 and 6P68, where small amounts of sodium calcium phosphate crystals ($2.4\ CaO \cdot 0.6Na_2O \cdot P_2O_5$) were found.

Table 2 summarizes the thermal expansion (α), softening (T_s), and transformation (T_g) temperatures of the glasses. The thermal expansions of the glasses cover a wide range, which includes the thermal expansion of Ti and Ti6Al4V ($9.5–10.5 \times 10^{-6}\ °C^{-1}$ at 400°C)[6] and Vitallium® ($\sim 14 \times 10^{-6}\ °C^{-1}$)[7], a Co-Cr alloy used in orthopedic implants. As expected, an increase of the silica content reduces α and increases T_s and T_g. It has been proposed that the thermal expansion and other properties of the glasses are roughly additive quantities and can be described using empirical fittings:[8-12]

$$y = \sum_{i=1}^{n} a_i p_i \qquad (1)$$

where, for a glass with *n* components, *y* is the property to be measured, p_i are the oxide

concentrations in weight % and a_i are empirical coefficients. Table 3 presents some of the coefficients proposed by different authors to predict the thermal expansion of silicate glasses. The coefficients for K_2O and MgO are always lower than those for Na_2O and CaO. Because the bioactivity of silicate glasses decreases with increasing silica content, K_2O and MgO were added to obtain bioactive glasses with low thermal expansion coefficients (close to that of Ti), so they can be used to enamel Ti-alloys without generating large thermal stresses. Additionally, glasses with lower silica content have lower softening points, so they can be used for enameling at temperatures below the α → β transformation of Ti.

Comparison of the data with different models showed that the empirical coefficients of Winkelmann and Schott,[11] English and Turner,[12] and Hall[10] (Table 4) give good fittings to the measured thermal expansions. The coefficient for P_2O_5 for each model was deduced using the thermal expansions measured in this work. Even though an increase of the silica content seems to be the more effective way to decrease thermal expansion, when comparing our results with those of Lockyer et al.[13] for glasses in the SiO_2-Na_2O-CaO-P_2O_5 system, it was clear to us that the addition of MgO and K_2O served to manipulate α as intended, and glasses with parallel composition and lower thermal expansion coefficients can be designed this way (Figure 1). The additions of MgO and K_2O also seemed to increase the softening point. However, T_s always remained well below the α → β transformation of Ti, as intended. It should be noted that it was not possible to use any of the proposed empirical coefficients to obtain a good fitting for Lockyer et al. data.[13]

The measured hardness and densities are of the order of those reported for silicate glasses.[9] The empirical model of Winkelmann and Schott,[11] (Table 2) seems to well

reproduce the experimental densities.

(2) Coating fabrication

Attempts to fabricate coatings with glasses 6P44-a, 6P44-b, and 6P53-a, as well as the original Bioglass® composition developed by Hench, always failed. These coatings crystallized almost completely even at the lowest firing temperatures (700°C), resulting in poor densification and lack of adhesion to the metal. The main crystalline phase present in the Bioglass® coatings was sodium calcium silicate ($Na_2Ca_2Si_3O_9$). Glasses with high alkali content typically have a lower onset of crystallization temperature[13] and are hygroscopic. As a result, the presence of [OH^-] ions on the surface of the glass powders promotes crystallization. FTIR clearly shows the presence of a [OH^-] hydration band in the glass powders stored for several weeks (Figure 2).

Because of the difference in thermal expansion, coefficients between the glass and the alloy thermal stresses are generated in the coating during fabrication, which can result in cracking and/or delamination. Figure 3 shows the range of glass compositions that can be used to prepare dense coatings that do not crack or delaminate on Ti and Ti6Al4V or Co-Cr alloys. Glasses with lower silica content have greater thermal expansion and can be used to coat Co-Cr, whereas SiO_2-rich glasses can be used to coat Ti-based alloys.

The systematic firing studies have revealed the optimum firing times and temperatures for the fabrication of the coatings. As an example, Figure 4 illustrates the effect of firing time and temperature on the coatings manufactured with glass 6P57 on Ti6Al4V and glass 6P50 on Co-Cr. Four regions can be distinguished. Below a critical time and temperature, the glass does not sinter. Then, at higher temperatures, the glass flows and

forms a dense layer. Some of these coatings delaminate when a 6.2 kg Vickers indentation is applied on the top surface. Nevertheless, a time and temperature region exists where the coatings are dense, exhibit good adhesion, and do not delaminate under indentation tests. In indentations performed at the glass/metal interface on polished cross sections of these coatings, cracks do not propagate along the interface, but instead tend to be driven into the glass. This is an indication of good glass–metal adhesion (Figure 5). At longer times and higher temperatures, excessive reaction between the glass and the metal generates brittle reaction layers and gas bubbles at the interface, which results in porous coatings with poor adhesion to the substrate. As expected, the optimum firing temperature is related to the softening point of the glass. Glasses with higher softening points required higher firing temperatures for the glass to flow and densify (Figure 6).

A TEM image of the 6P57/Ti6Al4V interface annealed at 800°C for 30 s is shown in Figure 7. An interfacial titanium silicide (Ti_5Si_3) layer, ~150 nm thick, can be observed. The Ti_5Si_3 layer is divided into two regions: a continuous nanocrystalline layer in contact with the alloy and, on top of it, a zone with isolated Ti_5Si_3 nanoparticles dispersed in the glass. The appearance of isolated particles on the TEM image can also result from the growth of elongated silicide grains, or dendrites, from the continuous layer into the glass. They may appear as isolated particles in the TEM samples where the dendrite intersects the cross section. On the other hand, a thin (~150 nm) continuous CrO_x layer can be observed at the interface between the Co-Cr alloy and the 6P50 coating (Figure 8). Both interfacial reaction layers get thicker (up to ~1 μm) after firing for longer times or at higher temperatures than optimum. The presence of thicker interfacial layers is accompanied by the massive formation of bubbles that degrade the integrity of the

coating. EDS analysis has shown the presence of P in the interfacial layer between the glass and Ti-based alloys in overreacted samples.

Following the experimental observations, the evolution of the glass/metal interfacial nanostructure can be summarized as follows. During heating, gas easily diffuses through the porous deposited glass coating and a thin oxide layer forms on the surface of the metal. Thin-film x-ray diffraction showed the presence of an oxide layer on substrates annealed at temperatures below the glass softening point (550–650°C).[14] At temperatures above the softening point of the glass, the glass layer sinters and flows. The inner glass/metal interface becomes sealed from the external atmosphere, and the glass dissolves the oxide layer and starts to react with the substrate. TEM showed the formation of a ~150 nm silicide or oxide layer in the samples fired under optimum conditions. These coatings did not delaminate during the indentation tests of adhesion.

The main reactions between the glasses and the alloys (formation of Ti_5Si_3 on Ti-based alloys and formation of chromium oxide on Co-Cr alloys) can be written as:

$$8Ti + 3SiO_2\ \{glass\} \rightarrow Ti_5Si_3 + 3TiO_2\ \{glass\} \quad (2)$$

$$5Ti + 3SiO_2 \rightarrow Ti_5Si_3 + 3O_2 \uparrow \quad (3)$$

$$Cr + 3/2\ Na_2O \rightarrow 1/2\ Cr_2O_3 + 3Na(g) \uparrow \quad (4)$$

$$Cr + 1/2SiO_2 \rightarrow CrO + 1/2Si \quad (5)$$

Additionally, several reactions have been proposed between Ti and P_2O_5 in the glass that result in the formation of Ti_4P_3.[15]

$$16Ti + 6P_2O_5 \rightarrow 4Ti_4P_3 + 15O_2\uparrow \quad (6)$$

$$9Ti + 3P_2O_5 \rightarrow 2Ti_4P_3 + 7O_2\uparrow + TiO \quad (7)$$

$$17Ti + 6P_2O_5 \rightarrow 4Ti_4P_3 + 14O_2\uparrow + TiO_2 \quad (8)$$

Most of these reactions result in the formation of gaseous products, which explains the presence of bubbles in overreacted samples.

In conventional enameling theory it is proposed that in order to achieve optimum glass/metal bonding, the glass in contact with the alloy should be saturated with the lowest valence oxide of the metal without the presence of interfacial layers. In this way, according to the theory, a transition region will form between the metallic bonding of the substrate and the ionocovalent bonding of the glass, providing a "continuity of electronic structure" that will result in good adhesion.[16-18] However, the lack of characterization of enamel interfaces at the nano-level precludes a complete confirmation of this theory. The result of this work suggests that optimum adhesion is achieved through the formation of nanostructured interfacial layers. For the coatings on Ti6Al4V, the bond between the thin silicide layer and the metal can be helped in part by the good lattice matching. Also, if Ti_5Si_3 dendrites grow into the glass, they can provide some mechanical interlocking that can contribute to the adhesion, as it has been proposed for other metal–ceramic systems.[19-20] It should be noted that, if the oxide formed in the surface of the substrate during heating is not completely dissolved and a thick oxide layer remains at the interface, the coating delaminates during cooling or during the indentation test. This is the case for those samples fired at temperatures below the optimum. The detrimental effect of thick interfacial oxide layers on adhesion has also been observed during fabrication of glass coatings on other metals such as Cu or Fe.[18-23]

(3) In vitro behavior

The XRD and SEM analysis of the samples immersed in SBF for 30 days has shown the presence of HA crystals precipitating on coatings with silica contents lower than 60 wt%. The apatite crystals have flake-like morphology with sizes in the range of 50–100 nm. The FTIRSM and EDS analyses are consistent with carbonated hydroxyapatite [HCA, $Ca_{10}(PO_4)_3(CO_3)_3(OH)_2$)] crystals that incorporate 1–5 wt% MgO into their structure (Figure 7). In polished cross sections, a Si-rich layer can be observed by EDS between the precipitated HA layer and the remaining glass (Figure 8). After 2 months in SBF, the apatite layer grew to a thickness of ~20 μm.

The observed behavior is consistent with a mechanism of apatite formation similar to that described by Hench for Bioglass®.[3] The steps involved are: (1) the exchange of Na^+ and K^+ from the glass with H^+ or H_3O^+ from solution, accompanied by the loss of soluble silica into the solution and the formation of silanols on the glass surface; (2) condensation and repolymerization of a SiO_2-rich layer on the surface; (3) migration of Ca^{2+} and PO_4^{3-} through the silica-rich layer forming a $CaO–P_2O_5$-rich film that incorporates calcium and phosphates from solution; and (4) finally, the crystallization of the amorphous calcium phosphate film to form an apatite layer. De Aza et al.[24] have pointed out that the increase in pH on the glass surface due to the ionic exchange between the labile cations Na^+, K^+, Ca^+, etc., is necessary for the partial dissolution of the silica-rich layer and the subsequent apatite precipitation.

The silica content of the glass plays a critical role. Low silica compositions have a more open network structure that facilitates ion exchange with the solution, resulting in faster glass corrosion and precipitation of apatite. There is a critical SiO_2 content above

which the coatings lose their ability to precipitate hydroxyapatite when soaked in SBF. In these coatings, the critical silica content is around 60 wt%, very similar to that reported for bulk glasses in the SiO_2-Na_2O-CaO-P_2O_5 system (which includes Bioglass®) and other related compositions prepared in a conventional way.[1-3]

(IV) Dip-coating of dental implants

Ethanol-based slurries were used to coat cylindrical implants by dip-coating. The average glass particle size was 13 ± 2 μm. In this preliminary research, use of additional organics in the slurries such as dispersants was avoided. Burning of organics can result in the formation of bubbles in the coating that cannot be eliminated during the short firing times required for Ti-based alloys. Continuous stirring was required during the dip-coating process to avoid settling of the glass powders. Suspensions with solid contents lower than 70 wt% resulted in irregular coatings with thickness <25 μm. However, by using suspensions with a solid content of 75 wt% and coating velocities of 1,000 mm/s, we were able to prepare ~100 μm thick coatings on cylindrical Ti dental implants with good adhesion to the alloy (Figure 9). The firing conditions are similar to those developed for flat substrates.

IV. Conclusions

A new family of glasses in the SiO_2-Na_2O-K_2O-CaO-MgO-P_2O_5 system has been formulated so that bioactive glass coatings can be prepared on orthopedic metallic implants by enameling. The partial substitutions of CaO by MgO and Na_2O by K_2O are required to match the thermal expansion of the coatings to that of Ti-based alloys. In that way, coatings with silica contents below 60 wt% that do not crack or delaminate can be prepared. This is an important requirement since glasses with silica contents greater than

60 wt% are no longer bioactive. During fabrication, control of the glass–metal reactions is a key step. Optimum adhesion is achieved through the formation of 100–200 nm thick interfacial layers. Care must be taken to prevent excessive reaction, which can result in loss of adhesion through the formation of a thick reaction layer accompanied by bubbles in the glass. The results of this study have been used to prepare glass coatings on commercial dental implants.

Acknowledgments

The authors would like to acknowledge Prof. K. Hiraga and Mr. B. Aoyagi for allowing us to use the ARM-1250 kV microscope and Drs. S Hata and K. Kaneko for TEM assistance. S. Fujino wishes to thank the Japanese Ministry of Education, Culture and Sciences for a fellowship given to him by the National Program of Fellowships for young researchers in foreign countries, 2000. S. Lopez-Esteban was partly supported by a Fulbright Grant and wishes to thank the Spanish Ministry of Education, Culture and Sports for financial sponsorship. This work is supported by the COE project in ISIR, Osaka University and the NIH/NIDCR grant 1R01DE11289 at Lawrence Berkeley National Laboratory.

References

1. Hench, L. L., Bioceramics. *J. Amer. Ceram. Soc.*, 1998, **81,** 1705-28.
2. Hench, L. L., Bioceramics: from concept to clinic. *J. Amer. Ceram. Soc.*, 1991, **74**, 1487-1570.
3. Hench, L. L. & Andersson, Ö., Bioactive glasses. In *An Introduction to Bioceramics*, eds L. L. Hench and J. Wilson. World Scientific, Singapore, 1993, pp. 41-62.
4. Hench, L. L. and O. Andersoon, *Bioactive Glass Coatings*. In *An Introduction to Bioceramics*, eds L. L. Hench and J. Wilson. World Scientific, Singapore, 1993, pp. 239-260.
5. The ASM Committee on Titanium and Titanium Alloys, Introduction to titanium and its alloys. In *Metals Handbook Vol 3. Properties and Selection: Stainless Steels, Tool Materials and Special-Purpose Metals*. American Society for Metals, Metals Park, Ohio, 1980, pp. 353-360.
6. The ASM Committee on Titanium and Titanium Alloys, Properties of titanium and titanium alloys. In *Metals Handbook Vol 3. Properties and Selection: Stainless Steels, Tool Materials and Special-Purpose Metals.* American Society for Metals, Metals Park, Ohio, 1980, pp. 372-412.
7. Severin, A., Brazing of cast iron and carbon steel. In *Metals Handbook Vol 6. Welding, Brazing and Soldering.* American Society for Metals, Metals Park, Ohio, 1993, pp. 906-923.
8. Jackson, M. J. & Mills, B., Thermal expansion of alumino-alkalisilicate and alumino-borosilicate glasses - comparison of empirical model. *J. Mat. Sci. Let.*, 1997, **16,** 1264-1266.
9. Morey, G. W., *The properties of glass*. *2d ed*, American Chemical Society. Monograph series, New York, 1954.
10. Hall, F. P., The influence of chemical composition on on the physical properties of glazes. *J. Amer. Ceram. Soc.*, 1930, **13**, 182.
11. Winkelmann, A. & Schott, O., Expansion Coefficients of Glazes. *Ann. Physik*, 1894, **51**, 730.
12. English, S. & Turner, W. E. S., Relationship between chemical composition and the thermal expansion of glasses. *J. Amer. Ceram. Soc.*, 1927, **10,** 122.
13. Lockyer, M. W. G., Holland, D. & Dupree, R., NMR investigation of the structure of some bioactive and related glasses. *J. Non-Crys. Sol.*, 1995, **188,** 207-219.
14. Gomez-Vega, J. M., Saiz, E. & Tomsia, A. P., Glass-based coatings for titanium implant alloys*, J. Biomed. Mat. Res.*. 1999, **46,** 549-559.
15. Donald, I. W., Review: preparation, properties and chemistry of glass and glass-ceramic-to-metal seals and coatings. *J. Mat. Sci.*,1993, **28**, 2841-2886.
16. King, B. G., Tripp, H. P. & Duckworth, W.W., Nature of adherence of porcelain enamels to metals, *J. Amer. Ceram. Soc.*, 1959, **42,** 504-525.
17. Pask, J. A. & Fulrath, R. M., Fundamentals of glasss-to-metal bonding: VIII, nature of wetting and adherence. *J. Amer. Ceram. Soc.*, 1962, **45**, 592-596.
18. Pask, J. A., From technology to the science of glass/metal and ceramic/metal sealing. *Ceram. Bull.*, 1987, **66**, 1587-1592.

19. Sherhod, C. & Stowell, M.J., Dual Phase Vitreous Enamels: Part 2 Adhesion of Vitreous Enamels on Steel. *Mat. Sci. Tech.*, 1989, **10**, 1044-1051.
20. Healy, J. H. & Andrews, A.I., The cobalt-reduction theory for the adherence of sheet-iron coats. *J. Amer. Ceram. Soc.*, 1951, **34,** 207-214.
21. Harrison, W. N., Richmond, J. C., Pitts, J. W. & Benner, S. G, Relation between roughness of interface and adherence of porcelain enamel to steel. *J. Amer. Ceram. Soc.*, 1953, **36**, 410-416.
22. King, R. M., Mechanics of Enamel Adherence VIII, Part – Studies in firing enamels under reduced pressure. *J. Amer. Ceram. Soc.*, 1933. **16,** 233-238.
23. Ashcroft, I. A. & Derby, B., Adhesion testing of glass ceramic thick films on metal substrates. *J. Mat. Sci.,* 1993, **28**, 2989-2998.
24. de Aza, P.N., Guitian, F., Merlos, A., Loratamayo, E. & de Aza, S, Bioceramics - simulated body fluid interfaces - pH and its influence of hydroxyapatite formation. *J. Mat. Sci. Mat. Med.*, 1996, **7**, 399-402.

Figure Captions

Figure 1. Comparison of the thermal expansion coefficients, (a) and the softening points (b) for glasses in the SiO_2-Na_2O-K_2O-CaO-MgO-P_2O_5 and SiO_2-Na_2O-CaO-P_2O_5 systems (the latter taken from Lockyer et al.[13]). Each line corresponds to glasses with the same silica content (in wt%). It can be observed that for parallel compositions, additions of K_2O and MgO serve to reduce the thermal expansion of the glass and increase the softening point.

Figure 2. FTIR analysis of Bioglass® powder stored for one month in air. The presence of a strong O-H hydration bands is clearly visible.

Figure 3. Compositional triangles showing the adequate composition ranges to coat Co-Cr and Ti-based alloys. All glasses have a constant 6 wt% P_2O_5 content.

Figure 4. Influence of firing time and temperature on the adhesion of coatings manufactured with glass 6P57 on Ti6Al4V and glass 6P50 on Co-Cr.

Figure 5. Vickers indentations at the glass 6P57/Ti6Al4V (1.2 Kg) and 6P50/Co-Cr (0.6 Kg) interfaces performed in ambient air. The cracks were driven towards the glass and the coating did not delaminate qualitatively indicating good glass-metal adhesion.

Figure 6. Relationship between the optimum firing temperature and the softening point of the glasses.

Figure 7. TEM image of the cross section of a 6P57 glass coating on Ti6Al4V annealed at 800°C for 30 sec.

Figure 8. TEM image and associated line analysis of the interface between glass 6P50 and a Co-Cr alloy after firing at 750°C for 30 sec.

Figure 9. SEM micrograph and associated EDS analysis of apatite crystals precipitated on a 6P57 coating after 30 days in SBF.

Figure 10. Elemental cross section analysis (SEM-EDS) of a 6P57 coating after 2 months in SBF. A ~20 μm thick apatite layer is visible on the 6P57 coating surface growing on a Si-rich region.

Figure 11. Coated titanium internal hexagonal cylinder implants (b) and corresponding SEM of a polished cross section (b). During firing the glass has flown establishing good contact with the rough implant surface.

Table 1. Glass compositions in weight and mol % (the latter between parenthesis). All glasses have a P_2O_5 content fixed at 6 wt % so they are named as 6P followed by their silica content.

	SiO_2	Na_2O	K_2O	CaO	MgO	P_2O_5
Bioglass®	45	24.5	0.0	24.5	(0.0)	6.0
	(46.1)	(24.3)	(0.0)	(26.9)	(0.0)	(2.6)
6P44-a	44.2	23.6	6.5	12.6	7.1	6.0
	(45.2)	(23.4)	(4.2)	(13.8)	(10.8)	(2.6)
6P44-b	44.2	17	4.6	18	10.2	6.0
	(43.9)	(16.4)	(2.9)	(19.2)	(15.1)	(2.5)
6P44-c	44.2	10.3	2.8	23.4	13.3	6.0
	(42.7)	(9.7)	(1.7)	(24.2)	(19.2)	(2.5)
6P50	49.8	15.5	4.2	15.6	8.9	6.0
	(49.8)	(15.0)	(2.7)	(16.7)	(13.3)	(2.5)
6P53-a	52.7	17.0	4.6	12.6	7.1	6.0
	(53.4)	(16.7)	(3.0)	(13.7)	(10.7)	(2.6)
6P53-b	52.7	10.3	2.8	18.0	10.2	6.0
	(51.9)	(9.8)	(1.8)	(19.0)	(15.0)	(2.5)
6P55	54.5	12.0	4.0	15.0	8.5	6.0
	(54.5)	(11.6)	(2.6)	(16.1)	(12.7)	(2.5)
6P57	56.5	11.0	3.0	15.0	8.5	6.0
	(56.3)	(10.6)	(1.9)	(16.0)	1(2.6)	(2.5)
6P61	61.1	10.3	2.8	12.6	7.2	6.0
	(61.3)	(10.0)	(1.8)	(13.5)	(10.8)	(2.5)
6P64	64.1	9.8	2.7	11.1	6.3	6.0
	(64.7)	(9.6)	(1.7)	(12.0)	(9.5)	(2.6)
6P68	67.7	8.3	2.2	10.1	(5.7)	6.0
	(68.4)	(8.1)	(1.4)	(10.9)	(8.6)	(2.6)

Table 2. Empirical coefficients proposed by several authors to calculate the thermal expansion and density of silicate glasses. The optimum coefficient for P_2O_5 has been deduced using the results presented in this work.

	Thermal expansion				**Density**
	Wilkeman and Schott[11]	English and Turner[12]	Hall[10]	Gilard and Dubrull[8]	Wilkeman and Schott[11]
SiO_2	2.67	0.5	1.4	0.4	2.3
Na_2O	33.33	41.6	38	51-0.33·p	2.6
K_2O	28.33	39.0	30	42-0.33·p	2.8
CaO	16.67	16.3	15	7.5+0.35·p	3.3
MgO	0.33	4.5	2	0	3.8
P_2O_5	0.35	0.24	0.36	0.59	2.55

Table 2. Measured thermal properties of the glasses and predicted values of the thermal expansion using different models (the thermal expansion was measured in the range 200-400 °C).

	α ($x10^{-6}x°C^{-1}$)	T_s (°C)	T_g (°C)	Winkelmann and Schott[11]	English and Turner[12]	Hall[10]	Gilard and Dubrull[8]
Bioglass®	15.1	557	511	15.6	15.9	15.8	11.9
6P44-a	15.6	503	449	15.1	16.4	15.7	12.3
6P44-b	13	560	516	13.3	13.9	13.5	13.5
6P44-c	11.3	599	527	11.5	11.5	11.3	14.6
6P50	12.2	560	522	12.4	12.7	12.5	12.4
6P53-a	12.9	565	530	12.6	12.9	12.8	11.4
6P53-b	11.5	608	531	10.8	10.5	10.6	12.6
6P55	11	602	548	11.2	11.1	11.1	12.0
6P57	10.8	609	557	10.7	10.3	10.5	11.5
6P61	10.2	624	564	10.1	9.5	9.8	10.5
6P64	9.1	622	565	9.7	9.0	9.4	9.8
6P68	8.8	644	565	9.0	8.0	8.6	9.1

Table 3. Measured Vickers hardness and densities for selected glasses. Calculated densities using Winkelmann and Schott coefficients[11] are also presented.

	Hardness (GPa)	Density (g/cm^3)	Calculated density (g/cm^3)
Bioglass®	5.75	2.71	2.58
6P44-a	5.35	2.62	2.59
6P44-b	5.85	2.61	2.64
6P44-c	6.3	2.68	2.69
6P53-a	5.6	2.61	2.56
6P53-b	6.2	2.7	2.61
6P55	5.6	2.63	2.57
6P57	5.75	2.62	2.56
6P61	5.7	2.71	2.53
6P68		2.48	2.48

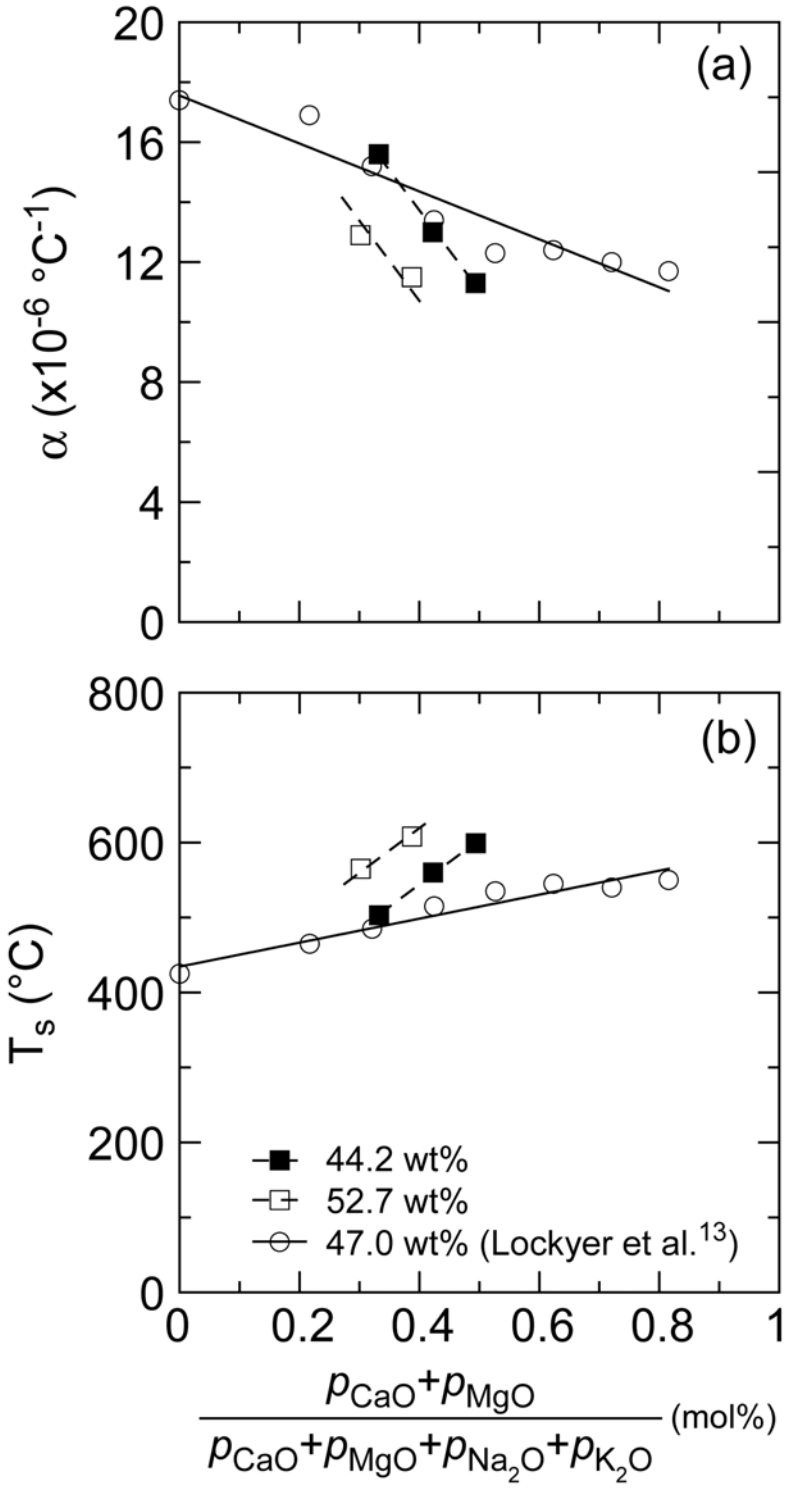
(a)
α (x10-6 °C-1)
20
16
12
8
4
0
(b)
Ts (°C)
800
600
400
200
0
0
0.2
0.4
0.6
0.8
1
44.2 wt%
52.7 wt%
47.0 wt% (Lockyer et al.13)
pCaO+pMgO
pCaO+pMgO+pNa2O+pK2O
(mol%)

Figure 1

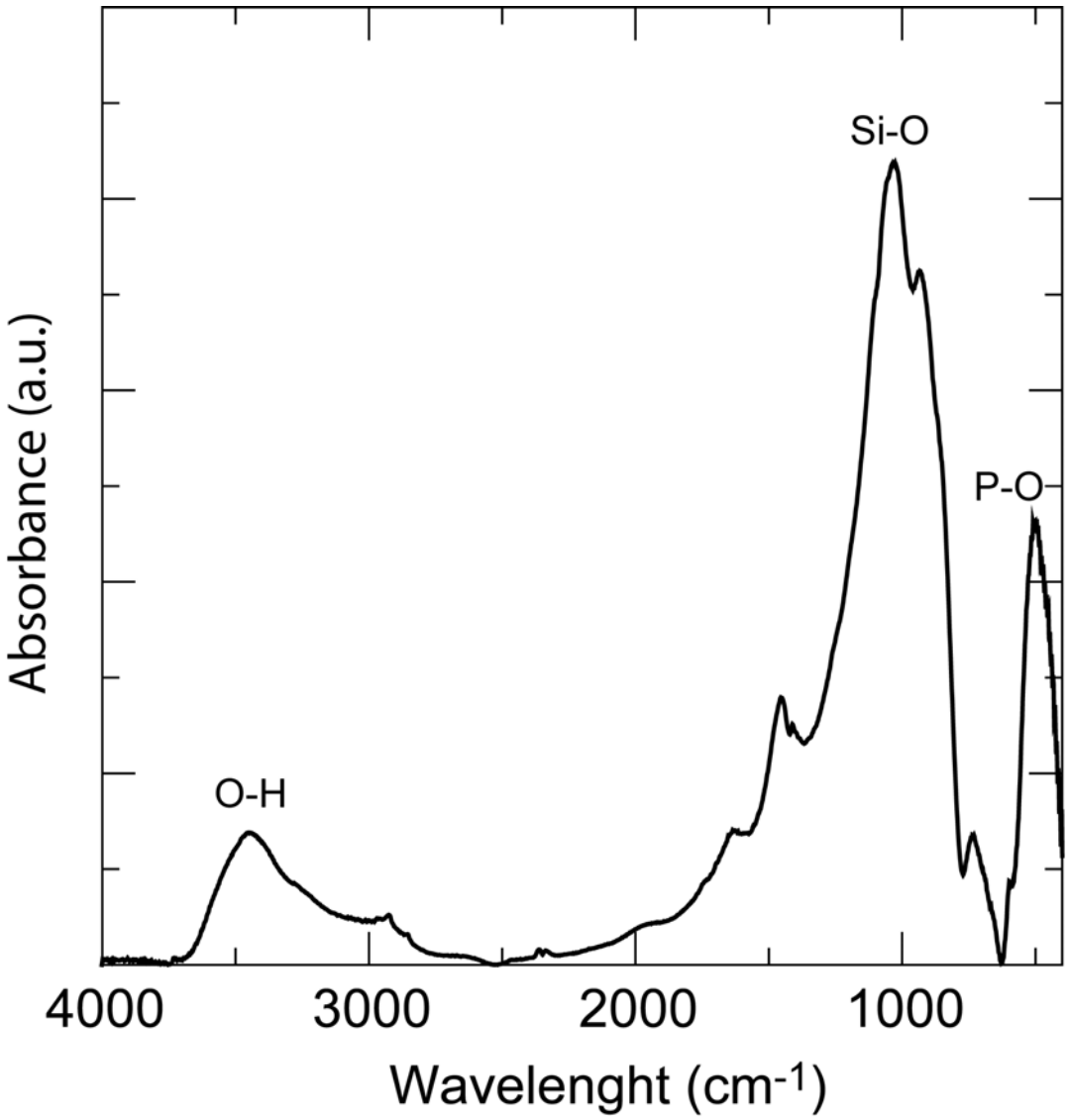

Figure 2

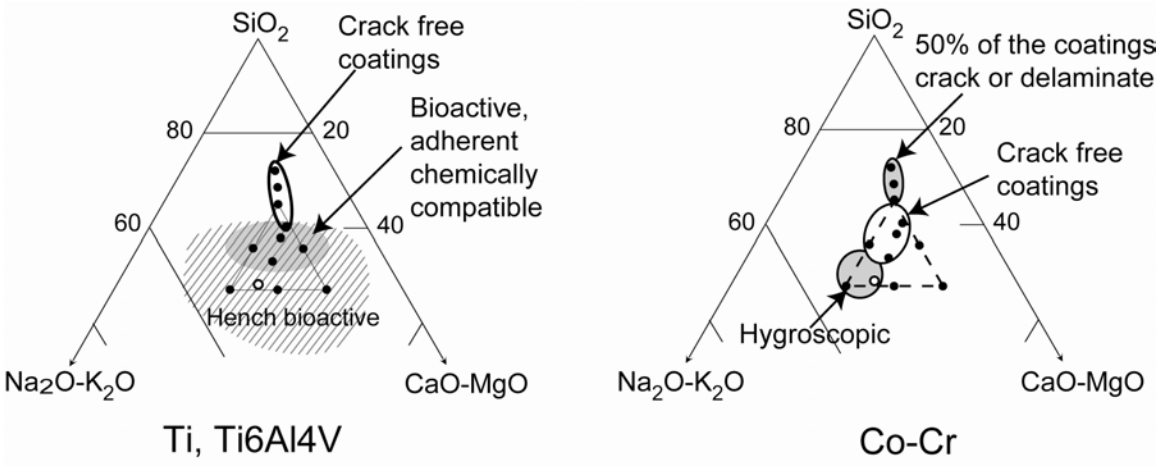

Figure 3

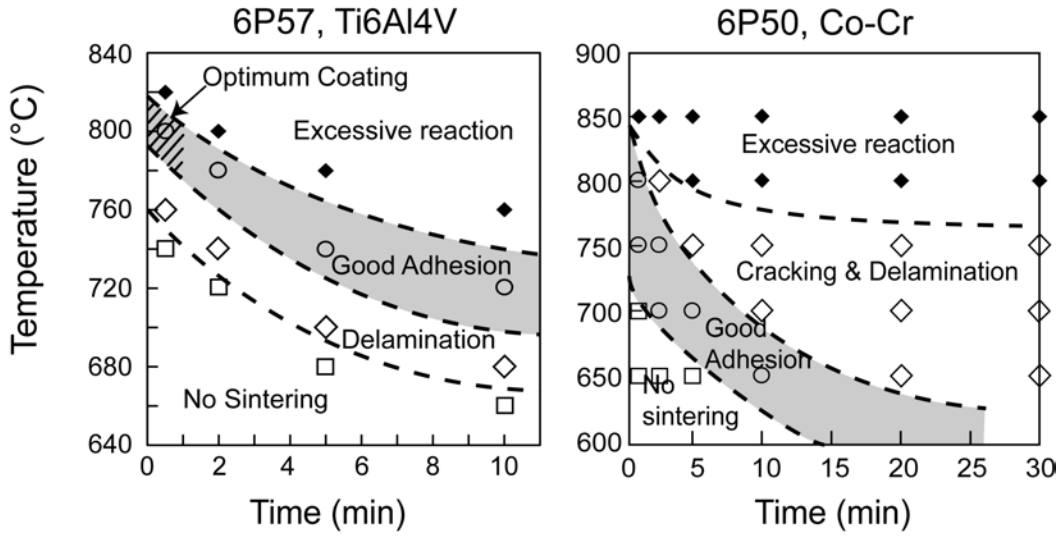

Figure 4

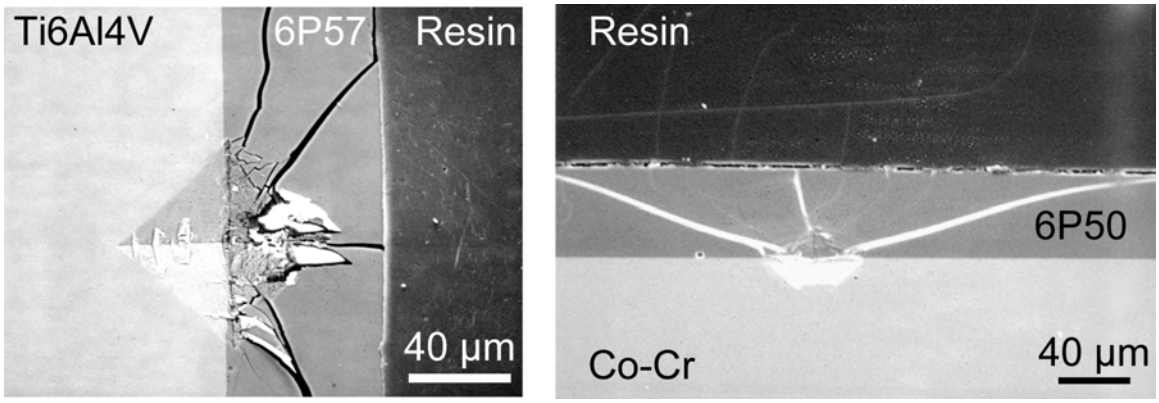

Figure 5

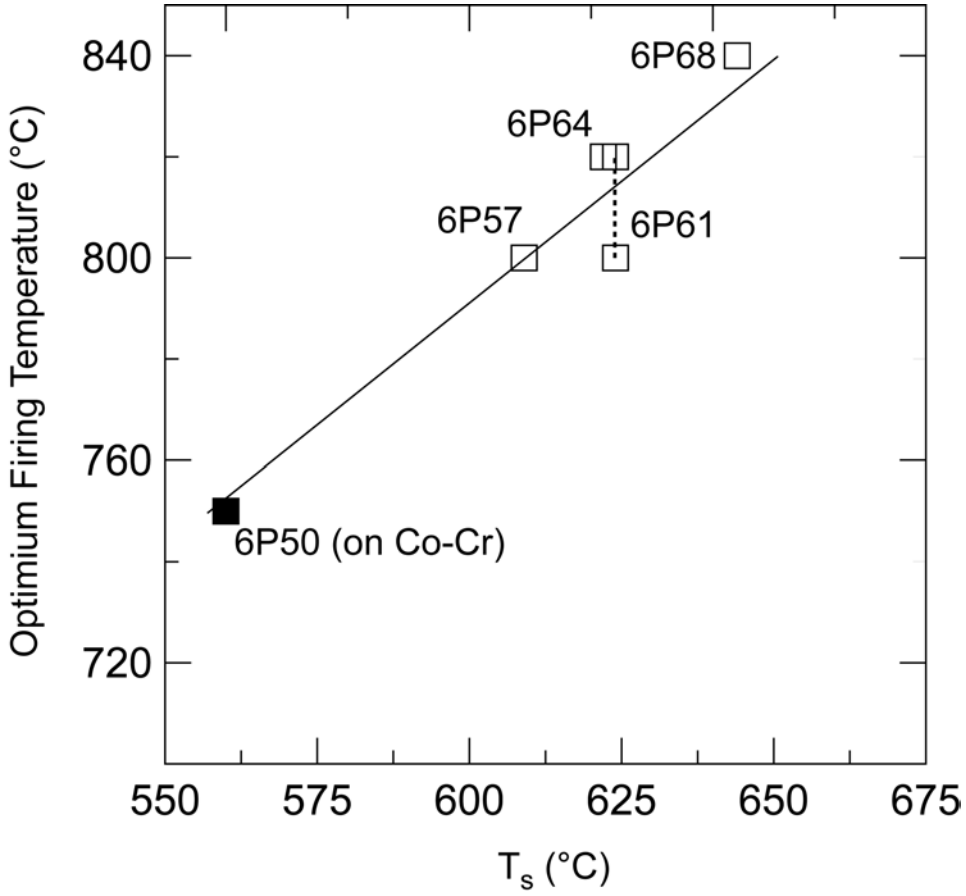

Figure 6

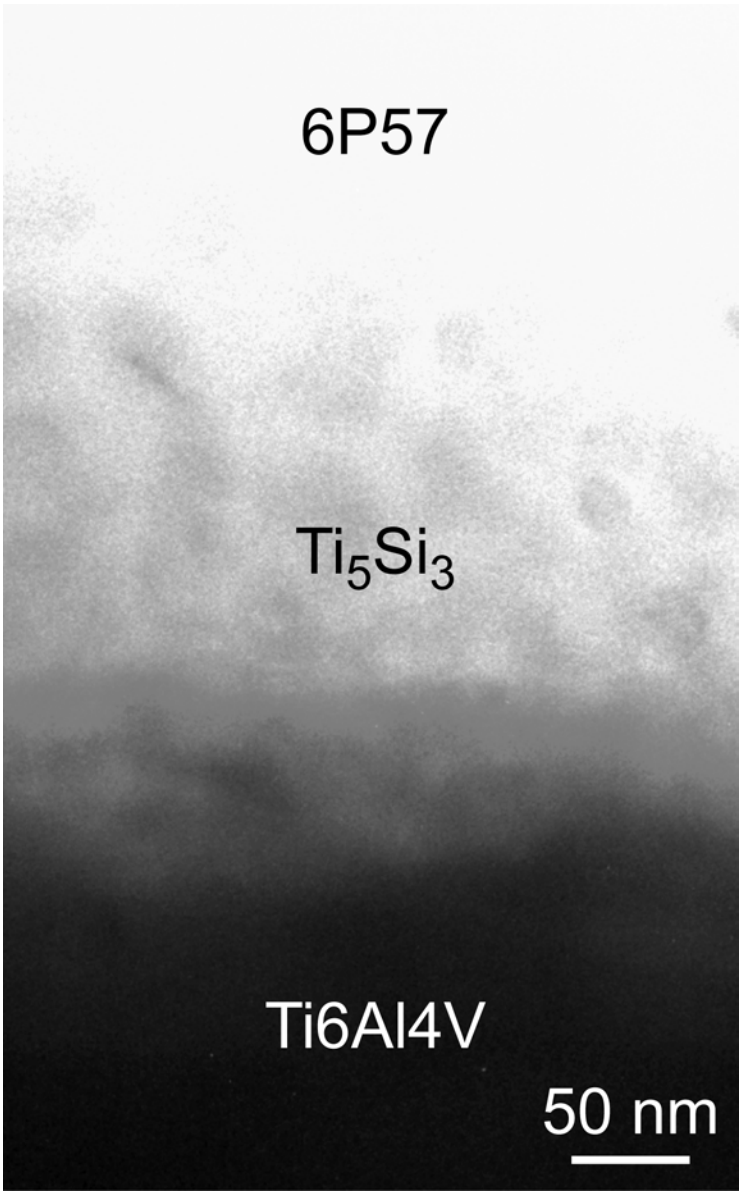

Figure 7

\

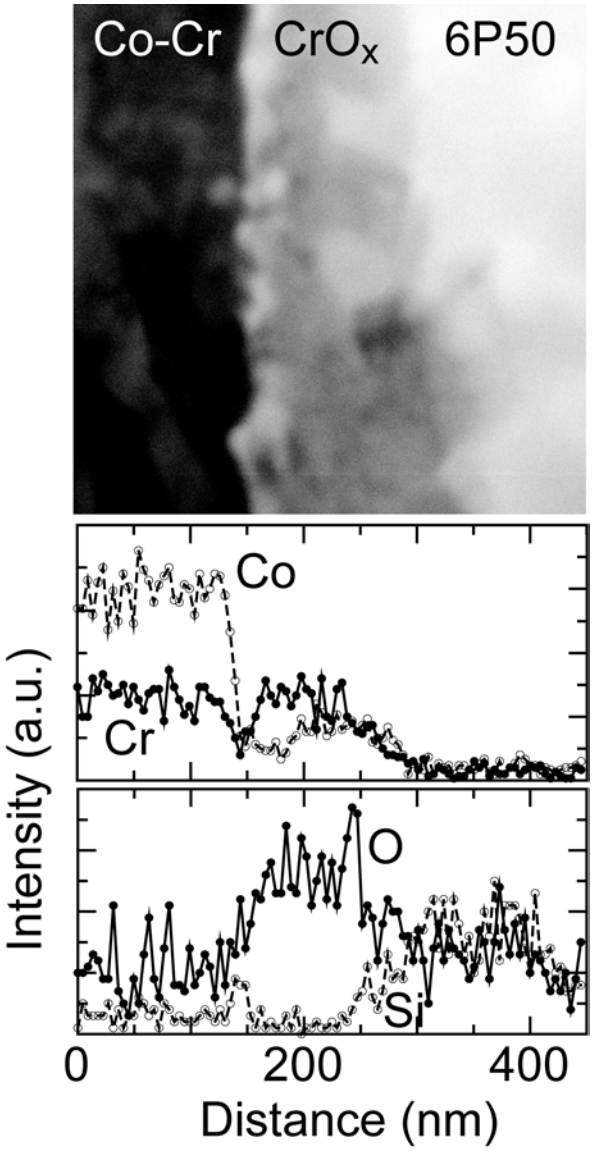

Figure 8

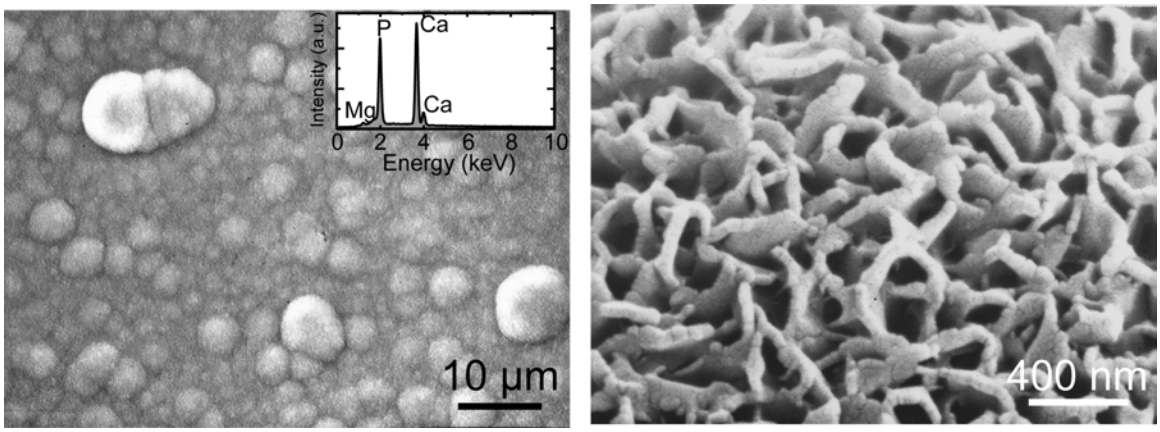

Figure 9

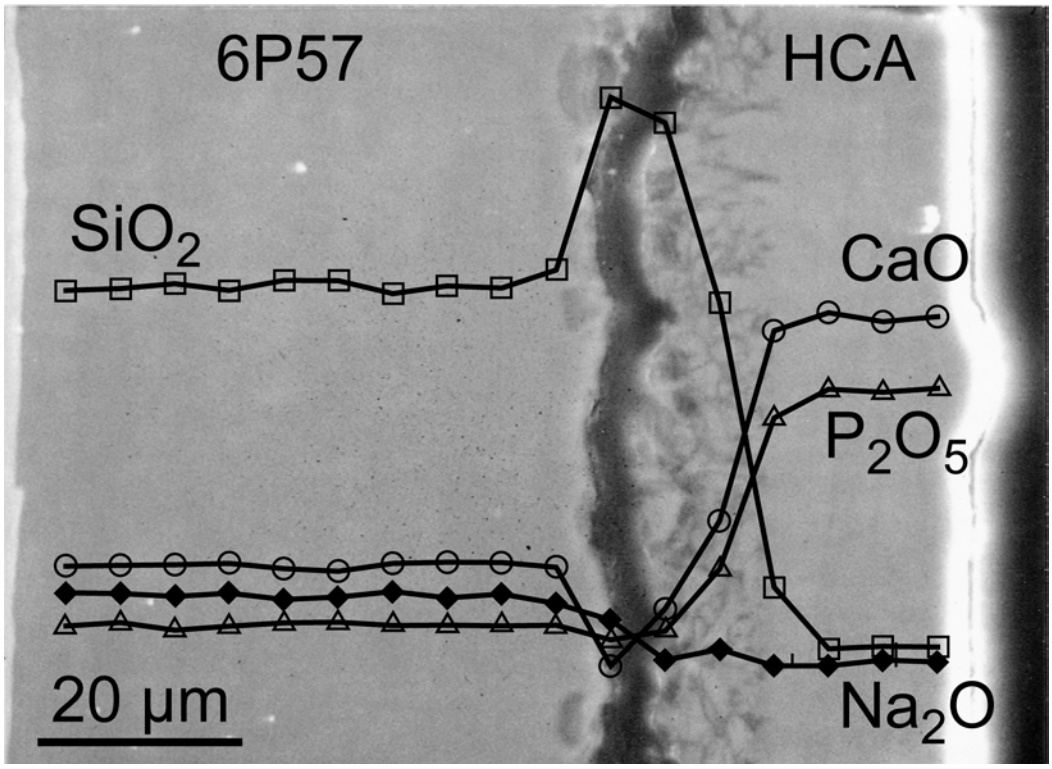

Figure 10

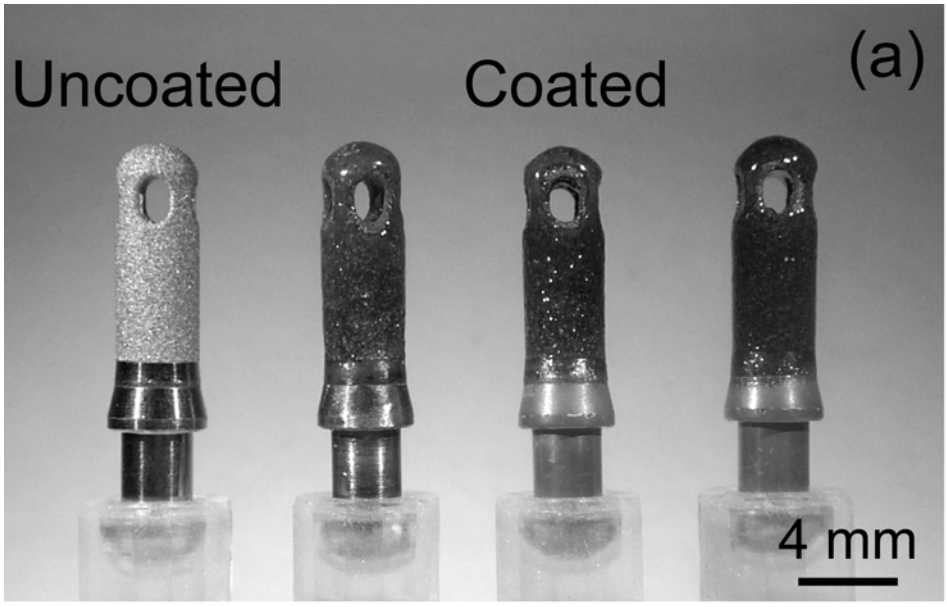

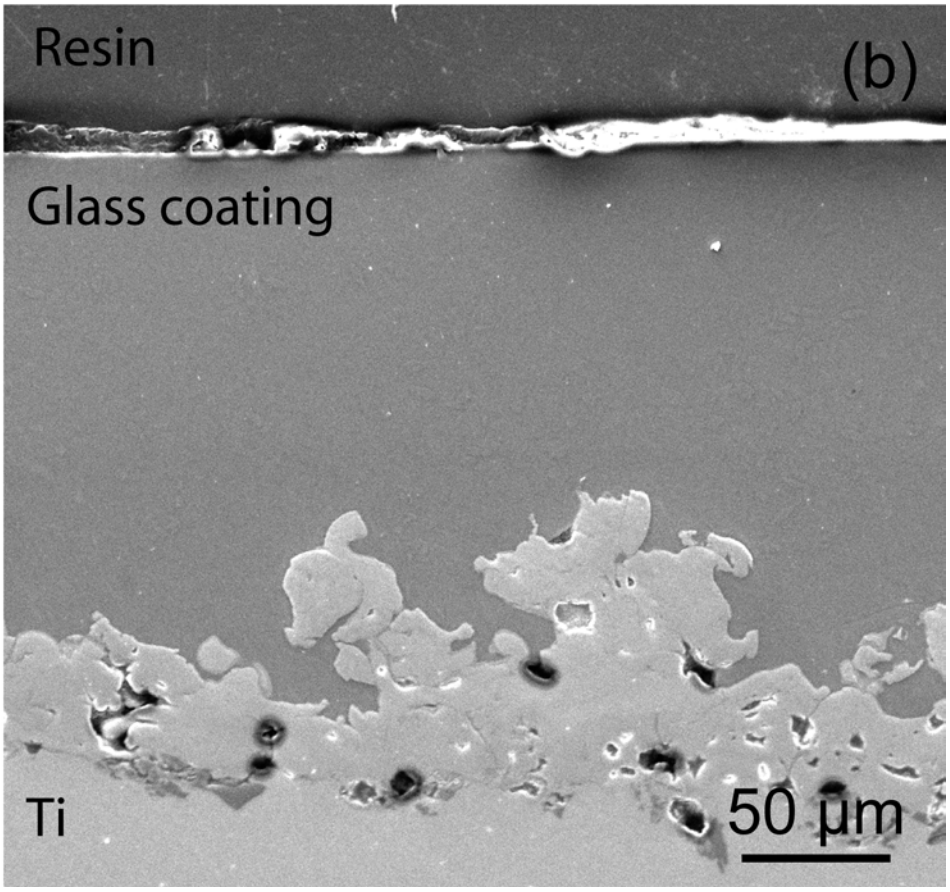

Figure 11